International Journal of Mass Spectrometry 524 (2026) 117609

Contents lists available at ScienceDirect

International Journal of Mass Spectrometry

journal homepage: www.elsevier.com/locate/ijms

Ion-specific kinetic energy distributions in MeV-SIMS: Insights into electronic sputtering processes

Boštjan Jenčič [a,*], Mirjana Sepahyar Lorentzen [b], Mitja Kelemen [a], Primož Pelicon [a]

[a] Jožef Stefan Institute, Jamova 39, 1000, Ljubljana, Slovenia
[b] Jožef Stefan Institute Postgraduate School, Jamova 39, 1000, Ljubljana, Slovenia

A B S T R A C T

Kinetic energy distributions of secondary ions produced by fast heavy primary ions (3 – 10 MeV ^{35}Cl, charge states 4+, 5+ and 7+) were measured to interpret the dynamics of ion desorption and formation under electronic stopping regime. All measurements were done on organic targets, such as various amino-acids and polymers, and were conducted using a reflectron mass spectrometer with a reflector electrode used as a tool to discriminate ions below the selected kinetic energy. Typical average kinetic energies of molecular ions range from 0.5 to 5 eV, with some smaller monoatomic ions or ion clusters, such as H^+ and H_2^+, exceeding 5 eV in average energy and exhibiting broader distributions. The type of cation was found to significantly affect kinetic energy distributions of organic molecules, with Ag adducts resulting in significantly lower kinetic energies and more pronounced "negative tailing" than e.g. protonated species. Systematic measurements across different target voltages ruled out gas-phase ion formation as a significant source of this tailing, which is more likely due to strong surface interactions or delayed ejection dynamics, specific to several secondary ion species. Additionally, fragmentation was found as a source of redistribution of internal energy into translational motion. On the other hand, the primary ion energy did not significantly affect the kinetic energy distributions of any analyzed species, thus confirming the dominance of the electronic stopping over nuclear stopping within the selected primary ion energy domain.

1. Introduction

Secondary ion formation in Secondary Ion Mass Spectrometry (SIMS) [1] arises from a complex sequence of processes initiated by primary ion impact, which leads to excitation, material ejection and ionization of sputtered species. While the common SIMS is dominated by nuclear stopping and collision cascades, sputtering induced by swift heavy ions in the MeV energy range domain occurs primarily within the electronic stopping regime. The fundamental physics of such electronic sputtering was extensively investigated in the 1980s and 1990s through Plasma Desorption Mass Spectrometry (PDMS) and accelerator-based heavy-ion desorption studies [2,3]. These works established that (for insulating and organic materials), ion emission correlates strongly with electronic energy loss along the ion track, while the contribution of nuclear stopping is minor.

Within this established framework, MeV-SIMS [4] [5–7] can be regarded as a modern implementation of swift heavy ion induced desorption, using focused accelerator beams and Time-of-Flight mass spectrometers for mass spectrometry imaging purposes. Compared to keV-SIMS, the desorption process is generally considered "softer", resulting in higher survival probabilities of large molecular ions [8–10]. Nevertheless, nuclear stopping still contributes at the levels of one percent (typically S_e ranges between 100 and 250 eV/Å, while S_n ranges between 1.4 and 3.4 eV/Å for 3-10 MeV Cl ions used in this work), and can influence fragmentation pathways and internal excitation of desorbed ions. Understanding how the deposited electronic energy is partitioned between translational motion, internal excitation and fragmentation remains an important question for MeV-SIMS and related techniques.

One important observable of desorption dynamics is the initial kinetic energy distribution (KED) of secondary ions [11]. KEDs have been widely investigated in keV-SIMS [12,13], gas cluster ion bombardment (GCIB) SIMS [14], MALDI [15], and PDMS [16–18], where they provide insight into energy transfer mechanisms, delayed emission and metastable decay [19,20]. For swift heavy-ion desorption, earlier studies reported characteristically low mean kinetic energies [21], however systematic measurements for molecular ions addressing the role of ionization pathway, adduct chemistry and extraction-field effects remain comparatively scarce.

In addition to the translational energy, the internal excitation of secondary ions plays a key role in determining their stability and fragmentation behavior. Previous research has shown that metastable decay rates depend strongly on the type of ionization [22] and on primary ion parameters [23], indicating that the internal energy content of emitted

* Corresponding author.
E-mail address: bostjan.jencic@ijs.si (B. Jenčič).

https://doi.org/10.1016/j.ijms.2026.117609
Received 19 November 2025; Received in revised form 2 March 2026; Accepted 14 March 2026
Available online 15 March 2026

ions is sensitive to both electronic excitation and desorption dynamics. Since translational and internal energies are both derived from the same deposited energy, a systematic study of kinetic energy distributions can provide complementary information on energy partitioning during the emission process.

Another open question concerns the origin of kinetic-energy deficits ("negative tailing") observed in some KEDs, where ions exhibit energies lower than the nominal extraction energy. Such features have been reported in various desorption techniques and may arise due to several factors.

The present work therefore investigates the kinetic energy distributions of secondary ions produced by MeV heavy-ion bombardment of organic films, focusing on amino acids and polyethylene glycol (PEG) with various alkali and Ag cation adducts. Using a reflectron ToF mass spectrometer with adjustable reflector potential, we obtain KEDs for a broad range of atomic and molecular ions. By varying the cationization pathway, target potential and primary ion energy, we aim to clarify how these parameters influence translational energy.

2. Methods

2.1. Sample preparation

All samples were purchased from SigmaAldrich. We analyzed several amino-acids, such as glycine, leucine and arginine, and also polymer polyethylene glycol (PEG) 600. In order to test the effect of the adduct, some analytes (arginine and PEG 600) were mixed with trifluoroacetate salts X-TFA, with X being Li, Na, K and Ag. The volume ratio of the mixture was 1:1 and it was dissolved in water at approx. 5 mg/mL. The droplets of approx. 5 μL were deposited on a silicon wafer (size of 1 × 1 cm^2) and spin-coated with 2000 rpm for 30 s, giving an approximate thickness of a film of 50-200 nm, depending on the analyte.

2.2. MeV-SIMS analysis

Analysis was performed at the 2 MV tandem accelerator at micro-analytical center of Jožef Stefan Institute, Ljubljana, Slovenia. Due to the compromise between the stopping power within the accessible energy range, and the focusing power of the magnetic quadrupole lenses, ^{35}Cl ions with energies between 2 and 10 MeV (50 to 400 keV/u) are typically used for MeV-SIMS. For these measurements, we have generated $^{35}Cl^-$ ions in the sputtering ion source, accelerated them in the tandem accelerator by voltages between 640 kV and 1.25 MV, and steered the ions with the selected charge state (4+, 5+ or 7+) towards the beamline. This resulted in corresponding energies of ions 3.2 MeV (S_e = 125 eV/Å, S_n = 3.4 eV/Å), 5.0 MeV (S_e = 170 eV/Å, S_n = 2.4 eV/Å) and 10.0 MeV (S_e = 250 eV/Å, S_n = 1.4 eV/Å), all of them possessing very similar magnetic rigidity, which made the transition between different beams faster.

All ion beams were focused to dimensions of approx. 15 × 15 μm^2, first by reducing the size of the slits (apertures) within the beamline, and finally by using triplet quadrupole magnetic lenses. The size of the beam was measured on a 200 periods per inch copper grid by positioning a channel electron multiplier (CEM) detector behind it. CEM was also used to measure the intensity of the primary ion beam.

2.3. KED measurement

Secondary ions were accelerated with a target voltage V_T of 3 kV to a Time-of-Flight mass spectrometer. The spectrometer has an installed Einzel lens, a reflection electrode, and two microchannel plate (MCP) detectors, one at the end of the linear stage, and the second at the end of the reflectron stage. Voltage on the reflection electrode V_R was used for the measurement of the initial kinetic energy distribution of the secondary ions. Due to several factors, such as a slight tilt of the reflection electrode, fringe fields and alignment tolerances, a careful calibration was needed in order to determine the V_C, a voltage where an ion with an energy of precisely e_0V_T would completely stop. The calibration was done for target voltages between 1 kV and 5 kV. The measured slope of the linear function V_C (V_T) was 1.003.

For each sample or primary ion energy, V_R was scanned from V_C - 20 V to V_C + 20 V. On the lower limit, the intensity of molecular peaks remained the same as the intensity with V_R = 0, while on the higher limit, the signal was reduced to the background only. Each measurement lasted 3-5 min, depending on the initial intensity for each analyte, and all measurements for the same analyte were of equal length.

The intensity of the peaks was determined through their integration and reducing the background. From this data, the secondary ion yield (Y) could be extracted. The function of $Y(V_R)$ has a monotonous, negative slope, and sees an accelerating decay beyond the point of V_C. Therefore, the function of $Y(V_R)$ was separated into a slow decay (for $V_R < V_C$) and fast decay (for $V_R > V_C$). For the fitting purposes, we applied an empirical function to the normalized secondary ion yield as:

$$Y(V_R) \,/\, Y_0 = \left[1 - k_1 (V_R - V_0)^2\right][1 - S(V_R)]$$

$$+ A e^{-[(V_R - V_c)/k_2]^2} S(V_R)$$

where k_1 is the decay rate at $V_R < V_C$, k_2 is the decay rate at $V_R > V_C$, A is the normalized intensity at V_C, and

$$S(V_R) = \frac{1}{1 + e^{-\left(\frac{V_R - V_c}{w}\right)}}$$

is the logistic transition function from slow to fast decay, where a parameter w defines the width of the transition region. Since the resolution of the power supplies was±0.5 V, this parameter was set to 0.5.

The function from Eq. (1) was fitted to the data, obtaining parameters k_1 , k_2 and A. Finally, a negative derivative of Eq. (1) is proportional to the KED.

3. Results

Fig. 1 displays the normalized secondary ion yield for various peaks – H^+, Li^+, $^{107}Ag^+$ and $(M + Ag)^+$, where M is PEG n = 14 (molecular weight without the adduct 632 Da). The maximum intensity of these peaks ranged between 2 × 10^4 and 1 × 10^5, where the relative error due to randomness was typically very low – less than 1 %. Samples exhibited the decrease in the secondary ion yield at as early as $V_R \approx V_c - 8$ V for the observed molecular peaks, so the parameter V_0 was set to V_C-10 V. The intensity of some samples (such as H^+ and Li^+) has no significant

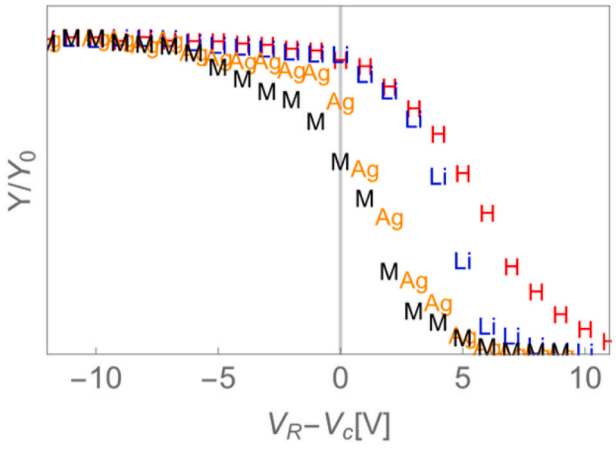

Fig. 1. Normalized secondary ion yield of secondary ions H^+, Li^+, Ag^+ and $[M + Ag]^+$ (M = PEG n = 14) as a function of V_R-V_C. Negative tailing is evident especially for the latter two species.

decrease up to V_R=V_C, which caused some irregularities with the derivatives of the fitted functions at the transition point. However, these deviations were found to be small and should be ignored. As can be observed in Fig. 1, the differences between the fitted parameters k_1, k_2 and A are quite clear.

The kinetic energy distributions were afterwards estimated as a derivative of the fitted function. The signal from both X-TFA mixtures of samples (arginine and PEG 600) was sufficient for all molecular peaks, and also for protonated molecular peaks for arginine (when prepared solely as solution in water). With unmixed PEG samples, the signal from the protonated peaks was significantly lower than with other adducts. The SIY on a protonated PEG n = 14 peak was measured at approx. 5×10^{-3}, which is one order of magnitude lower that the SIY of the same peak, cationized with Li, Na, K or Ag. This led to longer measurement times (10 min per point), which still yielded lower, but sufficient intensity of approx. 1×10^4 counts. The cumulative beam fluence on the spot was therefore considered as a possible source of error, however it was still in the range of 1×10^9 ions/cm^2, which is three orders of magnitude below the static limit measured for MeV-SIMS [24]. We tested this by starting the measurements at the lowest V_R and the proceeded to the highest (with the secondary ion yield decreasing), and then finalizing the measurements with measuring for V_R near the V_0 value again. The second measurement yielded the same result (±2%) as in the initial stages of the measurement procedure.

An overview of average kinetic energies for various ion species is presented in Table 1.

As can be deducted from the table, hydrogen ions have typically the highest average kinetic energies, exceeding 5 eV. The variation of their distributions was very low for different samples, including arginine and PEG in various matrices (mixtures with X-TFA), leucine and glycine. For all samples, the average kinetic energy range between 5.4 and 5.6 eV. Similarly, low variation of KED was observed in protonated arginine secondary ions, which were analyzed for all arginine related matrices, and also for Na^+ and Ag^+ peaks from Na- and AgTFA mixtures with PEG and arginine. On the other hand, Li^+ and K^+ exhibited slightly different characteristics in arginine and PEG samples, which cannot be explained by the measuring error alone. Generally, the role of the matrix was considered low, with some other common peaks, such as fragments $C_4H_8N^+$ (m/z = 70, common in arginine samples), and C_2H_4O (m/z = 45, common in PEG samples) also having similar KED for all matrices, but it was still relevant to some degree, as evidenced in Li and K.

Although this study focused more on positively charged secondary ions, a brief examination was also done on negative ions. Negative ions were found to have smaller average kinetic energy. While hydrogen does not exhibit any negative tailing in either charge state, average energies of molecular ions are significantly smaller in negative mode also due to the strong presence of negative tails. This applies for all three analyzed amino acids, arginine, leucine and glycine.

The role of the cation was studied in arginine and PEG samples. In both cases, the KED of $[M + X]^+$ peaks closely followed the KED of X^+ ions, when X = Li, Na, K (Fig. 2). With hydrogen, the KED of protonated peaks is much narrower, having lower average kinetic energy. On the other hand, for the case of Ag, the KED of molecular peaks differs significantly and exhibits much greater negative tailing, especially for PEG.

Average kinetic energies (KE) of measured molecular peaks range between 0.6 eV for $[M_{14} + Ag]^+$, and 4.6 eV for $[M_{14} + H]^+$ (Table 2). While for alkali cations and hydrogen the differences are small and no significant trends can be observed, the samples with Ag have noticeably lower average KE, which is primarily a result of more pronounced negative tailing. The phenomenon of negative tailing is commonly known [18] and is prominent especially in MALDI, where average KE for large proteins can shift significantly into the negative energy domain. The reasoning behind it is not yet clearly understood, but it is speculated that such onset is related to the gas phase formation of specific secondary ions, which can lead to the lower than nominal (e_0V_T) kinetic energy. However, other factors, such as sample charging, can also contribute to the energy deficit.

The intensity of negative tailing can be best presented through the parameter A (from Eq. (1)). Table 2 summarizes values of A for various ions. Evidently, the strongest negative tailing is always in samples with Ag, however with other adducts, negative tails occur less universally. For PEG samples, significant tailing was observed also with K, while with arginine samples, Li and also H have moderately pronounced negative tailing, rising significantly above the KED of sole adduct ion in the negative energy domain.

In several cases, the KEDs are not strictly single-peaked but exhibit a weak secondary maximum, which does not come from the transition of the fitted function, preceding the onset of the negative-energy tail, indicating that the observed distributions may contain contributions from more than one emission component.

Contrary to PEG, Arginine has two strong cation-binding sites, and can therefore also form $[M + 2X - H]^+$ secondary ions with high probability, if mixed with adduct containing matrices of proper concentration. The exemption is Ag, where the intensities of such peaks were too low measure reliably. The ratio between the intensities of $[M + X]^+$ and $[M + 2X - H]^+$ depends on the ratio between molecular and X-TFA concentrations, but with our samples, the two intensities were typically very similar for all alkali metals.

Although the KED of $[M + X]^+$ is very similar to the KED of X^+, the differences between KED of $[M + X]^+$ and $[M + 2X - H]^+$ peaks are apparent for all analyzed adducts. Fig. 3 demonstrates the differences between the KED of the two molecular peaks. The KED of $[M + 2X - H]^+$ is shifted towards lower kinetic energies, with more prominent negative tailing and lower reach in the positive energy domain. Such differences might be well explained by the universal energy loss of such ions. This may arise either from distinct gas-phase formation dynamics or from

Table 1
Average kinetic energies, and strength of negative tailing for various ion species. The measured kinetic energies are in good agreement with earlier measurements of emission under MeV heavy ion-bombardment, which reported weak substrate dependence and similar energy ranges of a few eV [25,26].

Ion species	Avg. KE [eV]	Neg. tailing
H^+	5.4-5.6	None
H^-	4.1	None
Li^+	4.1-4.6	Low
Na^+	3.5-4.0	None
K^+	2.6-4.1	Varies
Ag^+	1.9-2.0	Strong
Arg + H	3.4-3.5	Moderate
Arg -H	2.1	Strong
Gly + H	2.7	None
Gly – H	0.6	Strong
Leu + H	3.0	None
Leu – H	1.4	Strong
PEG + H (n 10-20)	4.2-4.6	None

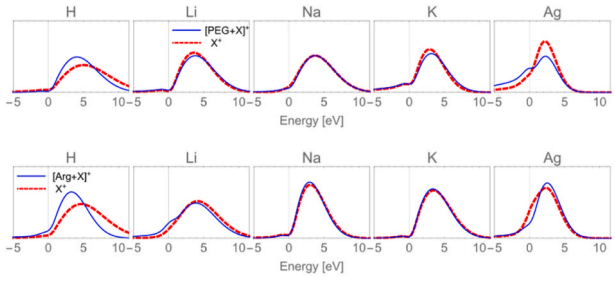

Fig. 2. Kinetic energy distributions of X^+ and $[M + X]^+$ secondary ions (X = H, Li, Na, K and Ag, M being PEG n = 14 or arginine). Plots exhibit clear correlation between X^+ and $[M + X]^+$ ions and demonstrate the onset of negative energy tails for several species.

Table 2
Average kinetic energies, parameters A (amount of secondary ions with positive KE) and k_2 (extension of positive KE) for X^+ an $[M+X]^+$ secondary ions (X = H, Li, Na, K and Ag, M = PEG n = 14).

X	H	Li	Na	K	Ag
Avg KE (Arg) [*eV*]	3.4	3.6	3.3	3.9	2.3
Avg KE (PEG) [*eV*]	4.6	4.1	4.1	2.7	0.6
A (Arg)	0.83	0.80	0.94	0.96	0.78
A (PEG)	0.97	0.93	0.92	0.80	0.52
k_2 (Arg) [*V*]	4.6	5.0	3.7	4.3	3.2
k_2 (PEG) [*V*]	5.3	4.6	4.8	4.0	2.9

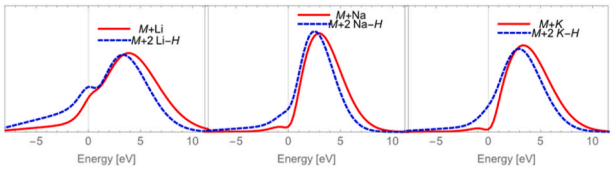

Fig. 3. Kinetic energy distributions of $[M+X]^+$ and $[M+2X-H]^+$ secondary ions for Li, Na and K (M = arginine). A shift in KED distribution can be observed for all three adducts.

enhanced electrostatic attraction to the sample surface.

KED measurements across different target potentials (V_T) were performed to clarify the onset of negative tailing and to understand the shift observed in the doubly cationized arginine peaks. By the gas phase formation hypothesis, one assumes, that a significant percentage of secondary ions, which are formed in such fashion, lose a certain amount of the nominal kinetic energy due to them not being formed precisely at the target potential. E.g. if the distance from the target to the nozzle of the spectrometer is 5 mm, and ions are formed at 5 μm [18] from the sample surface, then the lost potential is 0.1 % of the target voltage. This leads to a different KED when measuring with different target potentials, since the shift due to the gas phase formation is lower with lower target voltages.

The results in Fig. 4 show the distributions of Arg + H and Arg+2Na-H for various voltages. While the measured distributions of protonated arginine peak remain similar within the margin of error, the distribution of the doubly cationized arginine peak shift towards higher energies for higher target voltages. This result goes against the gas phase formation theory, where kinetic energy distributions should shift towards smaller values with an increase of target voltage. It is more likely that specific molecules have stronger bonding with the surface, and higher target voltages provide a more efficient separation with the lesser loss of kinetic energy.

The KED of various peaks within the same spectra varies significantly, and depends on the size of the secondary ion, and also on the fragmentation level of a specific secondary ion species. These variations can be best demonstrated on PEG samples, since they consist of three

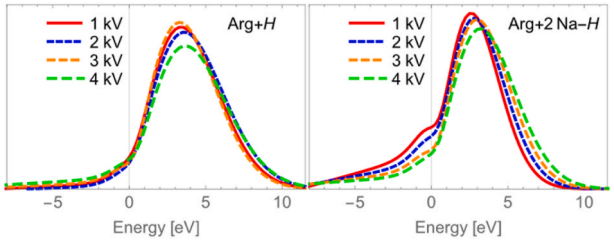

Fig. 4. Kinetic energy distributions of for protonated arginine (left) and doubly cationized arginine (right) peaks at target voltages of 1 kV, 2 kV, 3 kV and 4 kV. No significant differences in KED were observed for the protonated peak, while the distribution of the doubly cationized peak is shifted towards higher kinetic energies at higher target voltages.

different series of peaks: "A series" ($[M+X]^+$), "B series" ($[M+X-H_2O]^+$), and "C series" ($[M+X-H_2]^+$). The KED of the C-series could not be measured because the spectral peaks were broadened when the reflectron electrode potential was closely matched to the target voltage, resulting in interference from the more intense A-series signals. In contrast, the B-series ions were clearly resolved and exhibited a shifter KED relative to the A-series, as shown in Fig. 5.

Fig. 5 shows the intensities of secondary ions within the PEG 600+AgTFA spectra with a given kinetic energy. Here, the dominant molecular peaks are between m/z = 550 and 900, as marked in the picture, where the periodic nature of both A series and B series can be clearly observed. The map shows the differences between the KED of A series and B series, such as much more prominent negative tailing of A series, and broader distribution of B series with less intense maximums.

Average kinetic energies and the strength of negative tailing across the PEG spectra are presented in Fig. 6. Once again, the prominence of negative tails is represented through the parameter A. The separation between A series and B series can be clearly observed in both plots.

Hydrogen and its clusters (H_2 and H_3) exhibit the highest average kinetic energies, above 5 eV. In the low-mass region (m/z 0-100), both the average and most probably kinetic energies decrease systematically. Most species in this range are formed through direct physical ionization rather than protonation. Later, however, the trend ends, and clear arrangement of KED can only be observed for molecular peaks, where A series peaks have an average kinetic energy between 0.6 and 1.1 eV, and B series peaks are between 2.9 and 3.4 eV.

Varying the energy of ^{35}Cl primary ions between 3 and 10 MeV resulted in very minor differences between kinetic energy distributions of same peaks. Kinetic energy distribution for three peaks in the PEG 600 + Ag sample is presented in Fig. 7. The additional measurement with 5 MeV primary ion beam, which was done on a different sample, during a different beamtime slot and therefore under slightly different measuring conditions, such as beam intensity and beam resolution, exhibited good repeatability of the previously obtained (and discussed) results. All parameters remained within the margin for error. k_1 was measured at 0.27 V^{-2} (previously 0.29 V^{-2}), A was 0.50 (previously 0.52), and k_2 2.9 V (previously 2.9 V).

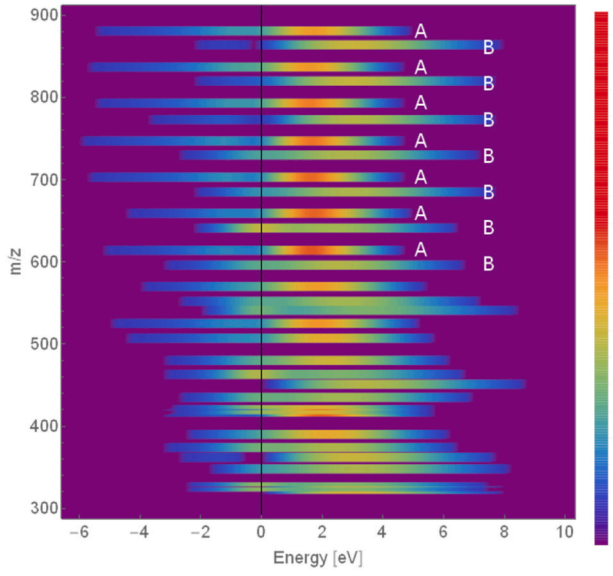

Fig. 5. KED map of the PEG + AgTFA spectra for mass range between 300 and 900. A visible difference can be seen between kinetic energies of A series ($[M+Ag]^+$) and B series ($[M+X-H_2O]^+$). For A series, most of the secondary ions seem to have kinetic energies between 1 and 3 eV, while for B series, the distribution is broader and spans between 2 and 6 eV. A series also has a much more prominent negative tailing.

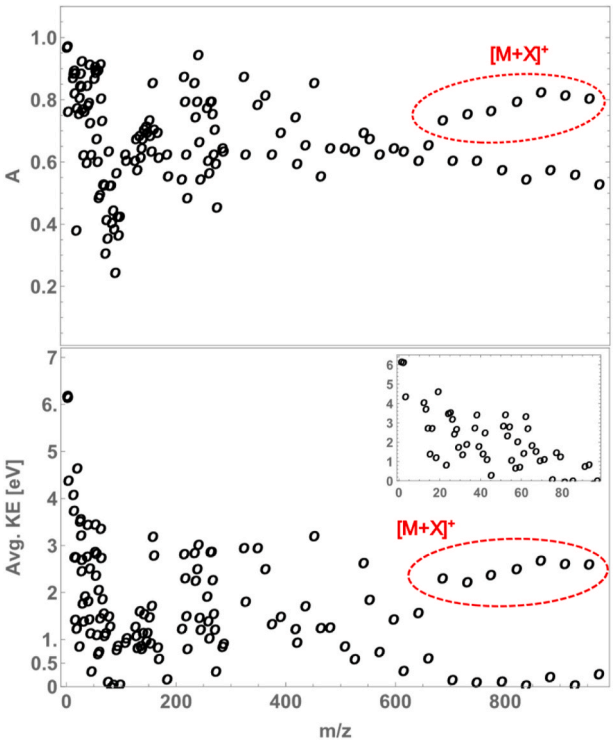

Fig. 6. Parameter A (above) and average kinetic energy (below) for various peaks in the PEG + AgTFA mass spectra.

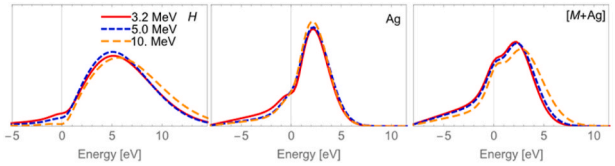

Fig. 7. KED of H^+, Ag^+ and $(M + Ag)^+$ of PEG (n = 14) for 3, 5 and 10 MeV primary ions. The distributions exhibit no significant differences, while the lower energy beams produce secondary ions with (on average) slightly more pronounced negative tailing and lower average KE.

While no significant differences can be observed for the KED of secondary ions under different primary ion energies, there are some minor distinctions, which can be observed. The strength of negative tailing decreases when the primary ion energy is increasing for all three peaks. Also, the parameter k_2 increases with increasing energy, resulting in slower decay on the positive kinetic energy side. This was evident only with H^+ and M+Ag peaks. Both of the two trends contribute to lowering the average kinetic energy of primary ions. However, these differences are very minor, and larger interval of primary ion energy should be included in analysis to confirm the trends. Additionally, the charge state of the primary ions might be another contributing parameter for these mild differences. However, our past analysis of SIY dependency on energy and charge state revealed energy to be the dominant parameter within the relatively small range of charge states provided [8].

4. Discussion and conclusion

The kinetic energy distributions (KEDs) of secondary ions in MeV-SIMS reveal that desorption is primarily driven by electronic stopping, resulting in soft, low-damage emission with limited fragmentation. Measured average kinetic energies range from 0.5 to 5 eV, reflecting modest translational energy transfer and energy partitioning governed by surface interactions and molecular structure. Such characteristics align well with the thermal spike model [27,28], where similar translational energies, quick decay at higher energies and strong species dependence are predicted. These observations are also consistent with earlier studies on insulating and organic films [21].

Hydrogen and its cluster ions (H_2^+, H_3^+) display the highest average kinetic energies, around 5.5 eV, with broad distributions indicative of diverse emission pathways near the sample surface. Heavier atomic cations and cationized molecular ions show lower average kinetic energies and, in some cases, pronounced negative tailing, reflecting stronger surface binding and partial energy loss during emission. The type of cation significantly influences the KEDs: cationized molecular ions closely follow the KED of the corresponding atomic cation for Li^+, Na^+ and K^+, whereas Ag^+ adducts exhibit broader distributions and more extensive negative tailing, indicative of stronger surface binding and more complex desorption dynamics.

Fragmentation plays an additional role in energy partitioning. In PEG samples, B-series ions exhibit higher kinetic energies than the parent A-series, indicating that internal energy released during partial fragmentation contributes to translational motion.

Negative tailing of certain molecular ions, particularly for Ag^+ adducts and doubly cationized arginine, can arise from multiple processes that are not distinguishable by KED shape alone. Besides gas-phase formation, several other mechanisms which result in energy deficits are reported in relevant MALDI and SIMS literature, such as collisions and field shielding in a dense desorption plume [13,29]. In the present data, varying V_T does not produce the shift expected for a dominant gas-phase formation of secondary ions, where the deficit scales with V_T. Instead, for $[M + 2X - H]^+$ the distribution shifts to higher apparent energies at higher V_T, suggesting the extraction-field dependent separation from the surface, and/or plume-related processes contribute more strongly than ion formation at a fixed reduced potential. We therefore interpret negative tailing as reflecting species-dependent surface/plume dynamics and fragmentation-related kinematics, while noting that further measurements would be required for a unique mechanistic assignment.

In addition to the lack of the expected V_T scaling for a fixed-distance gas-phase formation picture, the strong similarity between KED of X^+ and $[M + X]^+$ for X = Li, Na and K suggests that these ions share a common early desorption history and that formation occurs very close to the surface or within the film.

The appearance of a secondary maximum in some KEDs suggests a combination of at least two emission channels (prompt emission or delayed/fragmentation-related emission). Correlation/coincidence measurements between cations and cationized molecular ions would be an excellent future test regarding the origin of these species, however, this is beyond the scope of this work.

KEDs show minimal dependence on primary ion energy between 3 and 10 MeV, confirming that electronic stopping dominates over nuclear collisions in this regime. The small addition of nuclear stopping does not contribute significantly to the ejection dynamics, contrary to the case of fragmentation rate, where such range of primary ion energies results in large differences.

In conclusion, MeV-SIMS is characterized by soft, electronically driven desorption, where the kinetic energy of secondary ions is primarily governed by ion mass, cationization type and surface interactions. Hydrogen and its clusters show high, broadly distributed energies, whereas heavier cations and molecular adducts display lower energies and pronounced negative tailing. Fragmentation redistributed internal energy into translational motion, as observed in PEG samples. The lack of dependence on primary ion energy and the demonstration that gas-phase formation does not contribute noticeably to the tailing, suggest that surface binding and desorption dynamics are the dominant factor shaping KEDs. These findings provide mechanistic insight into energy partitioning and ion formation in MeV-SIMS, highlighting its utility for gentle, high-mass molecular analysis with minimal

fragmentation.

CRediT authorship contribution statement

Boštjan Jenčič: Writing – original draft, Visualization, Validation, Software, Resources, Project administration, Methodology, Investigation, Funding acquisition, Formal analysis, Data curation, Conceptualization. **Mitja Kelemen:** Writing – review & editing, Formal analysis.

Declaration of competing interest

The authors declare no conflict of interest for the paper entitled "Ion-Specific Kinetic Energy Distributions in MeV-SIMS: Insights into Electronic Sputtering Processes".

Acknowledgment

The authors acknowledge the financial support from the Slovenian Research and Innovation Agency (ARIS) (research core funding No. P1 – 0112, and basic projects J7-60126 and J7-70263) and Young Researcher Scholarship to M.S.L.

Data availability

Data will be made available on request.

References

[1] E.R. Amstalden van Hove, D.F. Smith, R.M. Heeren, A concise review of mass spectrometry imaging, J. Chromatogr. A 1217 (2010) 3946–3954.
[2] O. Becker, W. Knippelberg, K. Wien, Emission of non-metallic ions from a metal surface under heavy-ion bombardment, Physica Scripta 1983 (1983) 117.
[3] K. Wien, Fast heavy ion induced desorption of insulators, Nucl. Instrum. Methods Phys. Res. Sect. B Beam Interact. Mater. Atoms 65 (1992) 149–166.
[4] Y. Nakata, S. Ninomiya, J. Matsuo, Secondary ion emission from biomolecular thin films under ion bombardment, Nuclear Instruments and Methods in Physics B 256 (2007) 489–492.
[5] T. Raicu, M. Krmpotić, Z. Siketić, I. Bogdanović Radović, K. Sterflinger, D. Jembrih-Simburger, Beyond artists' colors: a spectral reference database for the identification of β-Naphthol and triarylcarbonium colorants by MeV SIMS, ACS Omega 9 (2024) 39573–39583.
[6] L. Jeromel, Z. Siketić, N. Ogrinc, P. Vavpetič, Z. Rupnik, K. Bučar, P. Pelicon, Development of mass spectrometry by high energy focused heavy ion beam: MeV SIMS with 8 MeV Cl7+ beam, Nucl. Instrum. Methods Phys. Res. B 332 (2014) 22–27.
[7] M. Krmpotić, D. Jembrih-Simbürger, T. Raicu, I. Bogdanović-Radović, M. Matijević, Z. Siketić, Matrix effects in MeV SIMS for modern pigment–binder systems: the influence of binder composition on SOP secondary molecular ion yield, Talanta 299 (2026) 129103.
[8] B. Jenčič, P. Vavpetič, M. Kelemen, P. Pelicon, Secondary ion yield and fragmentation of biological molecules by employing 35 Cl primary ions within the MeV energy domain, J. Am. Soc. Mass Spectrom. 31 (2020) 117–123.
[9] Y. Nakata, Y. Honda, S. Ninomiya, T. Seki, T. Aoki, J. Matsuo, Yield enhancement of molecular ions with MeV ion-induced electronic excitation, Appl. Surf. Sci. 255 (2008) 1591–1594.
[10] M. Brajković, M. Barac, I. Bogdanović-Radović, Z. Siketić, Dependence of megaelectron volt time-of-flight secondary ion mass spectrometry secondary molecular ion yield from phthalocyanine blue on primary ion stopping power, J. Am. Soc. Mass Spectrom. 31 (2020) 1518–1524.
[11] J. Laskin, C. Lifshitz, Kinetic energy release distributions in mass spectrometry, J. Mass Spectrom. 36 (2001) 459–478.
[12] B. Arezki, A. Delcorte, P. Bertrand, Kinetic energy distributions of molecular and cluster ions sputtered from self-assembled monolayers of octanethiol on gold, Nucl. Instrum. Methods Phys. Res. B 193 (2002) 755–761.
[13] A. Delcorte, P. Bertrand, Kinetic energy distributions of secondary molecular ions from thin organic films under ion bombardment, Nucl. Instrum. Methods Phys. Res. B 115 (1996) 246–250.
[14] A. Delcorte, C. Polenius, Mechanistic Insight into gas cluster-induced sputtering of Kilodalton molecules using kinetic energy distribution measurements, J. Phys. Chem. C 123 (2019) 19704–19714.
[15] D.R. Ermer, M. Baltz-Knorr, R.F. Haglund Jr., Intensity dependence of cation kinetic energies from 2,5-dihydroxybenzoic acid near the infrared matrix-assisted laser desorption/ionization threshold, J. Mass Spectrom. 36 (2001) 538–545.
[16] A. Albers, K. Wien, D. Dück, W. Treu, H. Voit, Secondary ion emission from dielectric films as a function of primary ion velocity, Nucl. Instrum. Methods Phys. Res. 198 (1982) 69–74.
[17] O. Becker, K. Wien, Energy of secondary ions desorbed from insulating films by MeV heavy ions as a function of projectile velocity, Nucl. Instrum. Methods Phys. Res. Sect. B Beam Interact. Mater. Atoms 16 (1986) 456–464.
[18] R.A. Zubarev, U.K. Abeywarna, P. Hakansson, P. Demirev, B.U. Sundqvist, Kinetic energies of secondary ions in MeV and keV particleinduced desorption, Rapid Commun. Mass Spectrom. 10 (1996) 1966–1974.
[19] I.S. Gilmore, M.P. Seah, Static SIMS: metastable decay and peak intensities, Appl. Surf. Sci. 144 (1999) 26–30.
[20] M. Bäumer, T. Adolphs, R.E. Peterson, H.F. Arlinghaus, B.J. Tyler, Strategies for minimizing interference from metastable water clusters in ToF-SIMS 3D imaging of frozen hydrated biological samples, J. Am. Soc. Mass Spectrom. 36 (2025) 2520–2530.
[21] G. Betz, K. Wien, Energy and angular distributions of sputtered particles, Int. J. Mass Spectrom. Ion Process. 140 (1994) 1–110.
[22] B. Jenčič, M. Kelemen, P. Pelicon, Cationization agent affects the stability of secondary ions in MeV-SIMS, Int. J. Mass Spectrom. 504 (2024) 117288.
[23] B. Jenčič, M. Vasić, Ž. Barba, M. Kelemen, P. Pelicon, Stability of MeV primary ion induced secondary ions, Int. J. Mass Spectrom. 487 (2023) 117037.
[24] M. Sepahyar Lorentzen, B. Jenčič, P. Vavpetič, P. Pelicon, The static limit in MeV secondary ion Mass spectrometry, J. Am. Soc. Mass Spectrom. 36 (2025) 900–905.
[25] C.C. de Castro, I.S. Bitensky, E.F. da Silveira, M. Most, K. Wien, Energy distribution of H+ ions desorbed from metal surfaces by MeV ion impact, Int. J. Mass Spectrom. Ion Process. 173 (1998) 1–15.
[26] M. Most, K. Wien, A. Brunelle, S. Della Negra, J. Depauw, D. Jacquet, M. Pautrat, Y. LeBeyec, H+ emission by MeV-ion impact: charge state dependence of energy and angular distributions, Nucl. Instrum. Methods Phys. Res. Sect. B Beam Interact. Mater. Atoms 168 (2000) 203–214.
[27] P. Sigmund, C. Claussen, Sputtering from elastic-collision spikes in heavy-ion-bombarded metals, J. Appl. Phys. 52 (1981) 990–993.
[28] M. Toulemonde, W. Assmann, C. Trautmann, F. Gruner, H.D. Mieskes, H. Kucal, Z. G. Wang, Electronic sputtering of metals and insulators by swift heavy ions, Nucl. Instrum. Methods Phys. Res. Sect. B Beam Interact. Mater. Atoms 212 (2003) 346–357.
[29] K. Dreisewerd, S. Berkenkamp, A. Leisner, A. Rohlfing, C. Menzel, Fundamentals of matrix-assisted laser desorption/ionization mass spectrometry with pulsed infrared lasers, Int. J. Mass Spectrom. 226 (2003) 189–209.